

Josephson coupling through one-dimensional ballistic channel in semiconductor-superconductor hybrid quantum point contacts

Hiroshi Irie,^{1,*} Yuichi Harada,¹ Hiroki Sugiyama,² and Tatsushi Akazaki¹

¹*NTT Basic Research Laboratories, NTT Corporation,
3-1 Morinosato-Wakamiya, Atsugi 243-0198, Japan*

²*NTT Photonics Laboratories, NTT Corporation,
3-1 Morinosato-Wakamiya, Atsugi 243-0198, Japan*

(Dated: April 23, 2014)

We study a superconducting quantum point contact made of a narrow $\text{In}_{0.75}\text{Ga}_{0.25}\text{As}$ channel with Nb proximity electrodes. The narrow channel is formed in a gate-fitted constriction of $\text{In-GaAs/InAlAs/InP}$ heterostructure hosting a two-dimensional electron gas. When the channel opening is varied with the gate, the Josephson critical current exhibits a discretized variation that arises from the quantization of the transverse momentum in the channel. The quantization of Josephson critical current persists down to the single-channel regime, providing an unambiguous demonstration of a semiconductor-superconductor hybrid Josephson junction involving only a single ballistic channel.

PACS numbers: 74.45.+c, 03.75.Lm, 73.63.Nm, 71.70.Ej

I. INTRODUCTION

The conductance of a ballistic point contact linking two reservoirs in thermal equilibrium is quantized in multiples of the conductance quantum $G_0 = 2e^2/h$.^{1,2} The origin of this phenomenon is the quantization of the transverse momentum in the narrow constriction. Strikingly, G_0 is independent of the parameters characterizing the contact, and the conductance is thus solely determined by the number of modes. Another interesting feature is that the contact has a finite resistance even though no scattering is assumed at the constriction. What happens if we replace the reservoirs with superconductors? This question was answered by Beenakker and van Houten a few years after the discovery of the conductance quantization³. They theoretically analyzed a superconducting quantum point contact (SQPC) made of a smooth and impurity-free superconducting constriction, and they showed that superconducting Josephson current is carried through the Andreev bound states which are phase-coherent discrete levels formed in each quantized mode. Since the energy spectrum of these levels is insensitive to the junction properties in the short-channel limit, the Josephson critical current I_c per mode is described by the junction-independent parameters as $I_0 = e\Delta_0/\hbar$ (Δ_0 is the superconducting gap). Note that I_0 has Δ_0 in its form in addition to the fundamental physical constants. In this respect, in contrast to the conductance quantization, the phenomenon is not universal. More theoretical work has been undertaken to take into account more realistic situations, such as a constriction longer than the superconducting coherence length, a Schottky barrier at the interface between the constriction and reservoirs, and elastic scattering in the constriction⁴⁻⁶. These analyses clarified that the step-like variation of I_c as a function of the mode number survives in a wide range of junction parameters, despite the fact that I_c per mode is sensitively altered by the

junction geometry and scattering process.

To prove the quantization of I_c , two types of experiments have been undertaken. The first uses a mechanically controllable break junction (MCBJ) made of two superconducting banks bridged by an atomically narrow constriction. By mechanically elongating or contracting the structure, the constriction's diameter, and hence the number of transport modes, can be tuned. A discretized change of the superconducting critical current with a step size comparable to $e\Delta_0/\hbar$ was observed in a Nb MCBJ⁷. Further study using different superconducting materials revealed that atomic valence orbitals constitute the current-carrying channels⁸. This finding indicates that it is difficult to manipulate either the number of transport modes or their transmission probabilities in a controlled way because these channels are extremely sensitive to the atomic configuration. Moreover, considering that even a single atom has several valence orbitals, isolating a single conducting channel is a challenging task for most metals except monovalent metals like Au⁹.

The second approach exploits the semiconductor-superconductor (Sm-Sc) hybrid structure. In a Sc/Sm/Sc junction, Josephson coupling is attained via Andreev reflection (AR) of quasiparticles confined in the Sm region. The transport properties of the quasiparticles, and hence the Josephson-junction (JJ) characteristics, can be controlled by means of the external electric field from a gate electrode. Quantum point contact (QPC) in a high electron mobility two-dimensional electron gas (2DEG)^{4,10} and gate-fitted nanowires¹¹⁻¹³ have been used as Sm materials to induce quantized conducting channels. In the former case, ballistic one-dimensional (1D) channels with almost perfect transmission can be formed with comparative ease because of their long mean free path. The number of channels is electrically tunable by a gate, which offers better controllability than an MCBJ. Takayanagi *et al.*¹⁰ experimentally demonstrated a 2DEG-based hybrid SQPC that utilizes

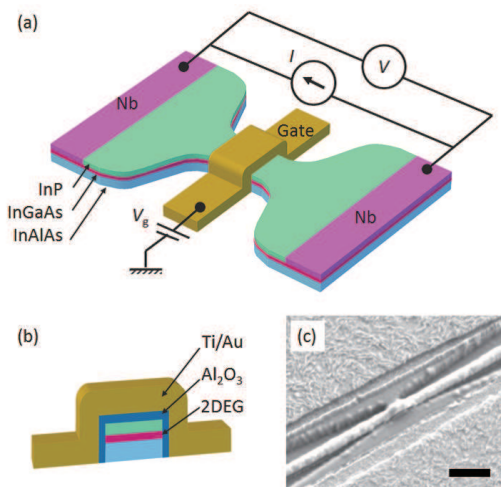


FIG. 1. (Color online) Schematic drawings of the (a) SQPC and (b) cross section of the wrap-gate QPC. (c) Scanning electron micrograph of a representative device tested. The black scale bar is 300 nm.

an InAs-based QPC with Nb proximity electrodes. They showed a stepwise change of both I_c and normal-state conductance G_n as a function of gate voltage. However, the quantization steps were vaguely visible, and the operation was limited to a few-channel regime ($n > 4$, where n is the number of 1D channels). Later, in a follow-up study¹⁴, it was found that I_c is excessively suppressed for $n < 3$, which hinders access to the single-channel operation. Other than the two reports above, there are no previous reports on this subject, and the realization of single-channel operation has been unattained so far. As for the nanowire-based hybrid SQPC, the quantized steps of I_c and G_n have not been observed in most devices using InAs nanowires^{12,13} except for the one using a Ge/Si core/shell nanowire with Al electrodes¹¹. In the present paper, we present a 2DEG-based hybrid SQPC that exhibits staircase variation of I_c from the multiple-channel regime down to the single-channel regime, which provides compelling evidence of the quantization of the Josephson critical current.

II. EXPERIMENT

The device structure of the SQPC studied is illustrated in Fig. 1. Similar to the SQPCs in the previous studies^{10,14}, it consists of a 2DEG-based QPC formed in a high-In-content InGaAs and two Nb electrodes in the vicinity of the QPC. In what follows, we describe the device structure, focusing on two major modifications to the SQPC studied previously.

Instead of the conventional finger-gate geometry, our QPC has a wrap-gate geometry, in which a narrow constriction made of an InP/In_{0.75}Ga_{0.25}As/InAlAs inverted-type high-electron-mobility transistor (HEMT)

structure¹⁵ is wrapped with an Al₂O₃ insulator and Ti/Au gate. The Al₂O₃ layer was formed by the atomic layer deposition technique, which provides low interface state density, resulting in a good gate controllability. Our previous study demonstrated a well-behaved QPC operation¹⁶, i.e., conductance steps with a constant stepheight of G_0 . More importantly, such clear conductance quantization is sustained even at temperatures down to 0.3 K and at zero magnetic field, where quantized steps are easily distorted due to scattering around the QPC^{17,18}. The geometry of the QPC used here is the same as the one in Ref. 16. The width and length of the narrow constriction are 120 and 200 nm, respectively. The length of the QPC is 80 nm, which is defined by the width of the gate electrode. Electron mobility μ_e and density n_s of the 2DEG at 1.9 K are 156,000 cm²/Vs and 1.9×10^{12} 1/cm², respectively. The calculated elastic mean free path $l_e (= \hbar\mu_e/e\sqrt{2\pi n_s})$ is 3.5 μ m. Electron effective mass m^* is obtained from the temperature dependence of the Shubnikov-de Haas oscillation as $0.043m_0$, where m_0 is the electron rest mass. Further information regarding to the wrap-gate QPC can be found in Ref. 16.

The Nb electrode, another key component of the SQPC, is fabricated by a lift-off process employing electron beam lithography. In order to achieve high AR probability, the Nb electrode has to directly touch the 2DEG, and the formation of a potential barrier at the interface should be avoided. A combination of coarse wet etching and subsequent *in situ* Ar plasma cleaning is carried out before Nb deposition. The former uses a phosphoric acid solution to selectively etch the InP layer on the InGaAs 2DEG layer. Thanks to the self-terminating process, the time required for the following *in situ* plasma cleaning can be minimized. The distance between the two Nb electrodes L_{ch} is chosen to be 300 nm. Since L_{ch} is much shorter than l_e , the SQPC is in the ballistic regime. When we discuss the superconducting properties of the SQPC, L_{ch} should also be compared with the coherence length in the 2DEG $\xi_0 (= \hbar v_f/\pi\Delta_0)$, where v_f and Δ_0 are the Fermi velocity and the superconducting gap). If $\Delta_{Nb} = 1.27$ meV is used for Δ_0 , which is calculated from the critical temperature of the Nb electrode ($T_c = 8.4$ K), we obtain $\xi_0 = 164$ nm, giving $L_{ch}/\xi_0 > 1$. This indicates that the SQPC is categorized as a long junction, in which multiple Andreev levels lie in the SQPC for each transport mode¹⁹. However, as we will discuss in the next section, Δ_0 will be replaced with a smaller value when a minigap is induced in the 2DEG via the superconducting proximity effect. In this case, the SQPC is in the short-channel regime ($L_{ch}/\xi_0 < 1$).

Current-voltage (I - V) characteristics of the SQPC were measured in a dilution refrigerator. Unless otherwise stated, all measurements were performed at 20 mK. A current source with a 200 k Ω load resistor was used for the bias sweep. The bias voltage V was measured by the four-terminal method using two independent contacts for each Nb electrode, which eliminated parasitic voltage drops other than that of SQPC. All the electrical lines in-

side the dilution refrigerator were twisted pairs equipped with a two-stage filter installed at the mixing chamber. The first stage comprises resistance-capacitance filters with a cutoff frequency of approximately 20 kHz. The second one consists of 2-m-long twisted pairs of constantan lines sealed tightly within folded copper tape. The latter filters out the high-frequency noise (frequency above 1 GHz), which is crucial for correctly evaluating the I - V curve of a JJ^{20,21}. In order to analyze the effects of the mode quantization, I - V curves were recorded at different values of gate voltage V_g . For each V_g , 20 measurements were performed to average out the statistical variation.

III. JOSEPHSON JUNCTION CHARACTERISTICS OF SQPC

Figure 2 shows typical I - V characteristics for three representative V_g values. All I - V curves show JJ characteristics with a superconducting branch at zero voltage. We define the current at which a finite voltage appears in a forward sweep as switching current I_{sw} . In a reverse sweep, the finite-voltage (resistive) state goes back to the superconducting branch at retrapping current I_r . The obtained I - V curves show a hysteresis; I_{sw} is not equal to I_r , which is commonly seen in Sc/Sm or Sc/metal hybrid Josephson junctions at temperatures much below the superconducting critical temperature. The hysteresis is most likely caused by heating in the resistive state. A direct measurement of normal-metal electronic temperature in an Al/Cu JJ demonstrates that the temperature increases once the JJ switches from a superconducting state to a resistive state which results in the reduction of I_r ²². Moreover, Sc/Sm hybrid JJs in general show a temperature independent I_r in the temperature range where its I - V curve shows hysteresis^{23–25}, indicating that I_r is suppressed in low-temperature limit due to the increased temperature by heating. As shown later in Fig. 4, our SQPC also shows a temperature independent I_r , supporting the idea that heating is the origin of the hysteresis in our SQPC. We note, however, that some controversial results have been reported regarding the origin of the hysteresis. A comparison between Sc/Sm/Sc junctions with and without a shunt capacitance indicates that the hysteresis is predominantly due to the underdamped nature of the JJ²³. Although the intrinsic quality factor of the junction itself is very small because of the small capacitive coupling between in-plane Sc electrodes, a stray capacitance could enhance the quality factor considerably, causing the underdamped behavior²⁰. For the underdamped JJ, we should be aware that a small fluctuation drives the JJ to switch to the resistive state below the intrinsic critical current, leading to a measured I_{sw} lower than the theoretical I_c . Nevertheless, we hereafter assume that our JJ is in the overdamped regime and that the hysteresis is caused by heating.

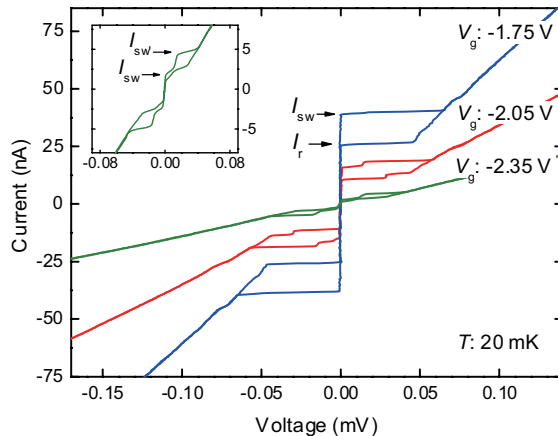


FIG. 2. (Color online) I - V characteristics of the SQPC taken at three representative values of V_g . The inset shows a magnified view of the I - V curve with $V_g = -2.35$ V.

With regard to the V_g dependence of the I - V curves in Fig. 2, both I_{sw} and I_r decrease with decreasing V_g , and the slope of the I - V curves in the resistive state simultaneously changes with V_g . This gate controllability in terms of superconducting properties is a unique feature of the Sc/Sm hybrid JJ. We also notice that the I - V curves for $V_g = -2.05$ and -2.35 V have an additional shoulder at the superconducting-to-resistive transition. A magnified view of the I - V curve for $V_g = -2.35$ V shown in the inset of Fig. 2 clearly display the shoulder at approximately 15 and 30 μ V for the forward and reverse sweep respectively. At elevated temperatures and under some V_g value, more than two shoulders appear in a single bias sweep (data not shown). These shoulders are caused by the ac Josephson effect^{26,27} due to an unintentionally formed cavity in the measurement system. As a result, the shoulders appear at integer multiples of 15 μ V (corresponding to resonant frequency of 7.3 GHz), and these positions are the same for all three samples tested. Although this effect seems to suppress the switching current of the first transition, we take it as I_{sw} as depicted in the inset of Fig. 2. Since this suppression occurs for I_{sw} below approximately 20 nA at 20 mK, it does not affect the I - V characteristics for most V_g values except near the pinch-off.

To study the effects of transport mode quantization, we show the V_g dependence of I_{sw} and differential conductance dI/dV in Figs. 3(a) and 3(b), respectively. The dI/dV is obtained by numerically differentiating an I - V curve at bias voltage $V = 0.2$ mV. The solid lines represent lines fitted using the following equations:

$$I_{\text{sw}} = I_{\text{sw}0} \sum_{n=1} T_n(V_g),$$

$$\left. \frac{dI}{dV} \right|_V^{-1} = \left[g_0 \sum_{n=1} T_n(V_g) \right]^{-1} + R_c, \quad (1)$$

where $I_{\text{sw}0}$ is the switching current per channel, g_0 is the conductance per channel, R_c is the contact resistance at the Nb/InGaAs interface, and $T_n(V_g)$ is the transmission probability of the n th channel. We presume here that each 1D channel contributes to the total switching current (or the conductance) by an equal amount of $I_{\text{sw}0}$ (or g_0) and the switching current (or the conductance) per channel is linearly dependent on the transmission probability. A saddle-point model is used to describe the potential landscape at QPC²⁸, providing $T_n(V_g) = \{1 + \exp[-2\pi(E_f(V_g) - E_n)/\hbar\omega_x]\}^{-1}$, where E_n is the lowest energy of the n -th subband, $\hbar\omega_x$ is the curvature of the saddle-point potential parallel to the current flow, and $E_f(V_g)$ is the V_g -dependent Fermi level. For $E_f(V_g)$, we use the relation with a constant dE/dV_g ($= 0.127$ eV/V)¹⁶. To calculate the fitted lines shown in the Figs. 3(a) and 3(b), we used the following set of numbers: $(I_{\text{sw}0}, g_0, R_c, \hbar\omega_x) = (10.3$ nA, 2.7 G Ω , 230 Ω , 5.9 meV).

The main finding of the present work is the clear step-wise variation of I_{sw} with respect to V_g in Fig. 3(a), by which we unambiguously prove the Josephson coupling through the quantized 1D channels. Furthermore, the reasonable fit with n -independent step height $I_{\text{sw}0} = 10.3$ nA (except for $n = 1$ and 2) demonstrates both an equal contribution of each 1D channel to I_{sw} and negligible intermixing between the channels, which is consistent with existing theories. The suppressed stepheights for $n = 1$ and 2 are presumably caused by the thermal activation escape because the Josephson coupling energy is comparable to the thermal energy of the bath temperature. The thermal activation escape in overdamped JJs causes the so-called phase diffusion²⁹ and results in a rounded switching in the I - V curve, which is indeed seen in the inset of Fig. 2. Despite the suppression of I_{sw} for the first channel, JJ behavior with an accompanying superconducting branch is clearly observed when V_g is set such that the SQPC holds a single ballistic channel (see the inset of Fig. 2 for the I - V curve).

In what follows, experimental $I_{\text{sw}0}$ is compared with theoretical I_c . In the simplest model assuming an SQPC in the short-channel limit ($L_{\text{ch}}/\xi_0 \ll 1$) with an ideal Sc/Sm interface, I_c is equal to $e\Delta_0/\hbar$ ^{3,4}. Given the influence of a finite channel length and a Schottky barrier at the Sc/Sm interface, I_c is modified as⁵

$$I_c = \alpha \frac{e}{\tau}, \quad (2)$$

with

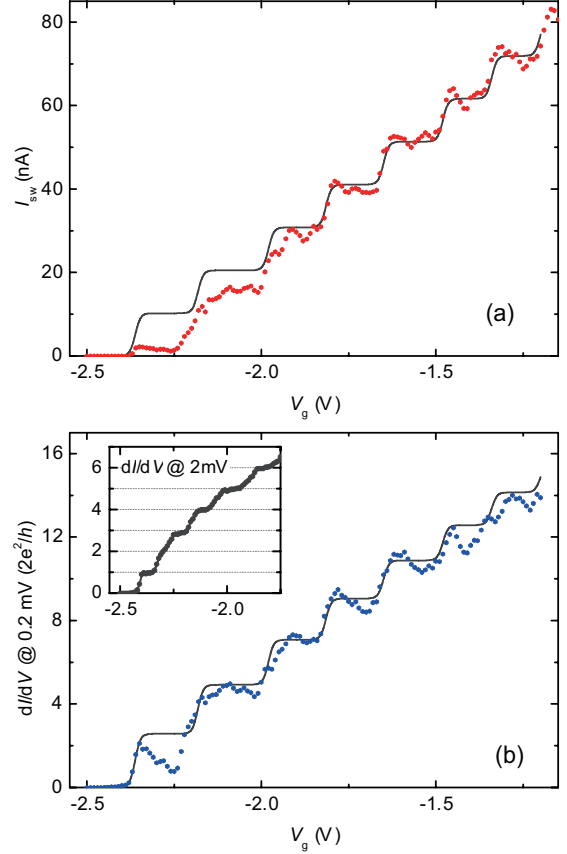


FIG. 3. (Color online) (a) V_g dependence of I_{sw} . (b) V_g dependence of dI/dV taken at $V = 0.2$ mV. For both (a) and (b), the dots represent experimental data, while the lines are fitted curves. Refer to the main text for the details of the fitting. The inset in (b) shows dI/dV taken at $V = 2$ mV. Note that the data in the inset were taken in a cool down cycle different from that in the main panels.

$$\tau = \frac{\hbar}{\Delta_0} + \tau_0 \left(\frac{2}{D} - 1 \right)$$

where α is a coefficient determined from the Fabry-Pérot-type interference effect due to the normal reflection at the Sc/Sm interface⁵, τ_0 is the time of flight of a quasiparticle in 2DEG L_{ch}/v_f , and D is the tunneling probability at the Sc/Sm interface. Note that Eq. (2) is reduced to the simplest form when $\alpha = 1$, $\tau_0 \rightarrow 0$ and $D \rightarrow 1$ are assumed. According to Ref. 3, the value of α oscillates as a function of V_g , as a result of the interference condition, within a range between 1 (constructive interference) and $D/4\pi$ (destructive interference). The value of D is determined from $D = 1/(1 + Z^2)$, where Z represents dimensionless barrier strength. Z can be roughly estimated from the relation $R_N = R_{\text{Sh}}(1 + 2Z^2)$, where R_N and R_{Sh} are the normal resistance and the

Sharvin resistance³⁰. Using a Sc/Sm/Sc junction with a wide constriction, we obtain $D = 0.59$ and $Z = 0.83$ for our SQPC. Plugging $D = 0.59$, $\Delta_0 = \Delta_{\text{Nb}} = 1.27$ meV, and $\tau_0 = 0.32$ ps (obtained with $L_{\text{ch}} = 300$ nm and $v_f = \frac{\hbar}{m^*} \sqrt{2\pi n_s} = 9.52 \times 10^5$ m/s) into Eq. (2) gives I_c of 125 nA for $\alpha = 1$ and 5.9 nA for $\alpha = D/4\pi = 0.047$. The experimental $I_{\text{sw}0}$ ($= 10.3$ nA) lies between these two values, and it can be explained by assuming a V_g -independent α with a value of 0.082. However, the absence of any pronounced peaks in our experimental data implies that no significant interference takes place and that α should be ~ 1 instead of small α value. If we use $\alpha = 1$, the model gives $I_c \sim 125$ nA for a single channel, which is one order of magnitude larger than the experimental $I_{\text{sw}0}$.

The large discrepancy can be resolved by taking into account the proximity layer at the 2DEG/Sc interface³¹, which has a pair potential called a minigap Δ_{mg} . To estimate Δ_{mg} , we fit the temperature dependence of I_{sw} using the theoretical model proposed by Kulik and Omelyanchuk (KO-2)³². In the model, the current-phase relation and critical current are described as $I_s(\varphi) = \frac{e\Delta_0}{\hbar} \sin(\varphi/2) \tanh\left[\frac{\Delta_0 \cos(\varphi/2)}{2k_B T}\right]$ and $I_c = \max[I_s(\varphi)]$, respectively. Figure 4 shows the temperature dependence of the experimental I_{sw} along with two calculated I_c 's using two different Δ_0 values. Note that I_{sw} is taken at $V_g = 0$ V, where roughly 15 channels are open, to make sure the Josephson coupling energy is larger than the thermal energy in the studied temperature range. Looking at Fig. 4, while the fit using $\Delta_0 = \Delta_{\text{Nb}} = 1.27$ meV clearly fails to reproduce the experimental data, the best fit is obtained when $\Delta_0 = 0.154$ meV, which we regard as Δ_{mg} . Now, $e\Delta_{\text{mg}}/\hbar$ gives $I_c = 38$ nA, still larger than but of the same order as $I_{\text{sw}0}$. Note that we use $e\Delta_{\text{mg}}/\hbar$ instead of Eq. (2) for calculating I_c because we do not know D , which could be drastically altered from 0.59 once the minigap is formed. This simplification overestimates I_c and could account for the remaining difference. Finally, we would like to point out that a similar Δ_{mg} value was obtained in a system similar to our SQPC from the density of state spectra of the proximity layer formed at the Nb/In_{0.8}Ga_{0.2}As interface²⁴.

In regard to the V_g dependence of dI/dV presented in Fig. 3(b), a clear stepwise change is also observed and the experimental data reasonably follow the fitted line. The striking part is that step height g_0 is equal to $2.7G_0$, which is larger than the quantized conductance G_0 . This enhancement is a consequence of the multiple ARs in the ballistic Sc/Sm/Sc junction³⁰. In contrast to a normal QPC, in which a limited number of transport modes are available under a finite voltage bias, the Andreev-reflected quasiparticles in the SQPC carry charges through fictitious electron or hole bands without exerting additional voltage. An SQPC is an ideal platform for demonstrating this effect because the conductance is determined not by the contact resistance at the Sm/Sc interface but by the number of 1D channels. Closely looking at the data in Fig. 3(b), we notice that

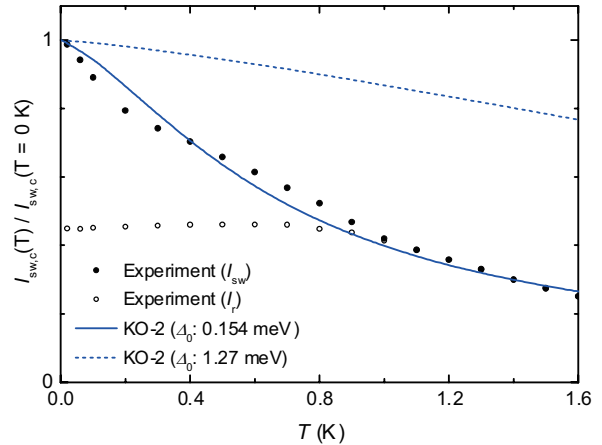


FIG. 4. (Color online) Temperature dependence of the switching current normalized by the value at 0 K. The solid and open circles are experimental data of I_{sw} and I_r , respectively. The solid and dashed lines are the curves calculated using the KO-2 model with $\Delta_0 = 0.154$ meV and $\Delta_0 = 1.27$ meV, respectively.

the experimental dI/dV deviates from the fitted line and exhibits a dip structure superimposed on the plateaus. This is most notable for the first plateau ($n = 1$), but other plateaus ($n = 4, 5, 6$) also exhibit the feature in a more subtle way. The unexpected dip is a characteristic feature in the low-bias regime. The inset of Fig. 3(b) shows dI/dV - V_g at 2 mV, in which the anomalous dip structure is flattened and conventional conductance quantization in units of G_0 is recovered. Since the charge transport is governed by the AR in the low-bias regime, these results indicate that the AR probability changes with V_g (or the position of the Fermi level in the QPC). The origin of this anomalous behavior is not clear, and further study is necessary to elucidate it.

IV. CONCLUSION

A Sc/Sm hybrid SQPC made of an In_{0.75}Ga_{0.25}As QPC with Nb electrodes is examined. The quantization of I_c is demonstrated by the staircase variation of I_{sw} . The staircase variation persists down to the single-channel regime, providing the first unambiguous demonstration of a Josephson junction with a single ballistic channel using Sc/Sm hybrid SQPCs. Although this quantized critical current has already been reported, the results presented in this paper prove it in a much clearer fashion. Beyond the experimental proof of quantized I_c , the realization of SQPC, especially single channel operation, opens up interesting possibilities for the application in quantum information processing. A pair of Andreev levels in a single channel SQPC forms a doublet state that can be utilized as a quantum bit³³. Recently,

a spectroscopy analysis of the Andreev levels in an Al-based MCBJ was performed, and its phase-dependent energy levels were successfully demonstrated²⁷. The studied SQPC allows us to precisely control the channel number, which is an advantage in realizing the Andreev level qubits.

ACKNOWLEDGMENTS

This work was supported by the "Topological Quantum Phenomena" (No. 22103002) Grant-in Aid for Scientific Research on Innovative Areas from the Ministry of Education, Culture, Sports, Science and Technology (MEXT) of Japan.

-
- * irie.hiroshi@lab.ntt.co.jp
- ¹ B. J. van Wees, H. van Houten, C. W. J. Beenakker, J. G. Williamson, L. P. Kouwenhoven, D. van der Marel, and C. T. Foxon, *Phys. Rev. Lett.* **60**, 848 (1988).
 - ² D. A. Wharam, T. J. Thornton, R. Newbury, M. Pepper, H. Ahmed, J. E. F. Frost, D. G. Hasko, D. C. Peacock, D. A. Ritchie, and G. A. C. Jones, *J. Phys. C*: **21**, L209 (1988).
 - ³ C. W. J. Beenakker and H. van Houten, *Phys. Rev. Lett.* **66**, 3056 (1991).
 - ⁴ A. Furusaki, H. Takayanagi, and M. Tsukada, *Phys. Rev. Lett.* **67**, 132 (1991); *Phys. Rev. B* **45**, 10563 (1992).
 - ⁵ N. Shchelkachev, *JETP Lett.* **71**, 504 (2000).
 - ⁶ N. M. Chitchev, G. B. Lesovik, and G. Blatter, *Phys. Rev. B* **62**, 3559 (2000).
 - ⁷ C. J. Muller, J. M. van Ruitenbeek, and L. J. de Jongh, *Phys. Rev. Lett.* **69**, 140 (1992).
 - ⁸ E. Scheer, N. Agraït, J. Cuevas, A. Yeyati, B. Ludoph, A. Martin-Rodero, G. Bollinger, J. van Ruitenbeek, and C. Urbina, *Nature (London)* **394**, 154 (1998).
 - ⁹ E. Scheer, W. Belzig, Y. Naveh, M. H. Devoret, D. Esteve, and C. Urbina, *Phys. Rev. Lett.* **86**, 284 (2001).
 - ¹⁰ H. Takayanagi, T. Akazaki, and J. Nitta, *Phys. Rev. Lett.* **75**, 3533 (1995).
 - ¹¹ J. Xiang, A. Vidan, M. Tinkham, R. M. Westervelt, and C. M. Lieber, *Nat. Nanotechnol.* **1**, 208 (2006).
 - ¹² Y. Doh, J. van Dam, A. Roest, E. Bakkers, L. Kouwenhoven, and S. De Franceschi, *Science* **309**, 272 (2005).
 - ¹³ T. Nishio, T. Kozakai, S. Amaha, M. Larsson, H. A. Nilsson, H. Q. Xu, G. Zhang, K. Tateno, H. Takayanagi, and K. Ishibashi, *Nanotechnology* **22**, 445701 (2011).
 - ¹⁴ T. Bauch, E. Hürfeld, V. M. Krasnov, P. Delsing, H. Takayanagi, and T. Akazaki, *Phys. Rev. B* **71**, 174502 (2005).
 - ¹⁵ The actual layer structure is, from the bottom to the surface, an undoped $\text{In}_{0.52}\text{Al}_{0.48}\text{As}$ buffer (200 nm), a $\text{Si } 4 \times 10^{18} \text{ cm}^{-3}$ doped layer (6 nm), an undoped $\text{In}_{0.52}\text{Al}_{0.48}\text{As}$ spacer (10 nm), a composite 2DEG layer consisting of $\text{In}_{0.53}\text{Ga}_{0.47}\text{As}/\text{In}_{0.75}\text{Ga}_{0.25}\text{As}/\text{In}_{0.53}\text{Ga}_{0.47}\text{As}$ (2.5/8/5 nm), an undoped $\text{In}_{0.52}\text{Al}_{0.48}\text{As}$ layer (3 nm), an undoped InP surface layer (5 nm).
 - ¹⁶ H. Irie, Y. Harada, H. Sugiyama, and T. Akazaki, *Appl. Phys. Express* **5**, 024001 (2012).
 - ¹⁷ T. Schäpers, V. A. Guzenko, and H. Hardtdegen, *Appl. Phys. Lett.* **90**, 122107 (2007).
 - ¹⁸ P. Ramvall, N. Carlsson, I. Maximov, P. Omling, L. Samuelson, W. Seifert, Q. Wang, and S. Lourduos, *Appl. Phys. Lett.* **71**, 918 (1997).
 - ¹⁹ T. Schäpers, *Superconductor/Semiconductor Junctions* (Springer, 2001).
 - ²⁰ P. Jarillo-Herrero, J. van Dam, and L. Kouwenhoven, *Nature (London)* **439**, 953 (2006).
 - ²¹ L. C. Mur, C. J. P. M. Harmans, J. E. Mooij, J. F. Carlin, A. Rudra, and M. Ilegems, *Phys. Rev. B* **54**, R2327 (1996).
 - ²² H. Courtois, M. Meschke, J. T. Peltonen, and J. P. Pekola, *Phys. Rev. Lett.* **101**, 067002 (2008).
 - ²³ V. M. Krasnov, T. Bauch, S. Intiso, E. Hürfeld, T. Akazaki, H. Takayanagi, and P. Delsing, *Phys. Rev. Lett.* **95**, 157002 (2005).
 - ²⁴ F. Deon, V. Pellegrini, F. Giazotto, G. Biasiol, L. Sorba, and F. Beltram, *Phys. Rev. B* **84**, 100506 (2011).
 - ²⁵ T. Schäpers, A. Kaluza, K. Neurohr, J. Malindretos, G. Creclius, A. vanderHart, H. Hardtdegen, and H. Luth, *Appl. Phys. Lett.* **71**, 3575 (1997).
 - ²⁶ M. Levinsen, *Appl. Phys. Lett.* **24**, 247 (1974).
 - ²⁷ L. Bretheau, Ç. Ö. Girit, H. Pothier, D. Esteve, and C. Urbina, *Nature (London)* **499**, 312 (2013).
 - ²⁸ M. Büttiker, *Phys. Rev. B* **41**, 7906 (1990).
 - ²⁹ V. Mel'nikov, *Physics Reports* **209**, 1 (1991).
 - ³⁰ M. Octavio, M. Tinkham, G. E. Blonder, and T. M. Klapwijk, *Phys. Rev. B* **27**, 6739 (1983).
 - ³¹ B. A. Aminov, A. A. Golubov, and M. Y. Kupriyanov, *Phys. Rev. B* **53**, 365 (1996).
 - ³² I. O. Kulik and A. N. Omel'yanchuk, *Sov. J. Low. Temp. Phys.* **3**, 459 (1977); **4**, 142 (1978).
 - ³³ A. Zazunov, V. S. Shumeiko, E. N. Bratus', J. Lantz, and G. Wendin, *Phys. Rev. Lett.* **90**, 087003 (2003).